

Intrinsic mixed state topological order in a stabilizer system under stochastic decoherence

Yoshihito Kuno,¹ Takahiro Orito,² and Ikuo Ichinose^{3,*}

¹Graduate School of Engineering science, Akita University, Akita 010-8502, Japan

²Institute for Solid State Physics, The University of Tokyo, Kashiwa, Chiba, 277-8581, Japan

³Department of Applied Physics, Nagoya Institute of Technology, Nagoya, 466-8555, Japan

(Dated: October 21, 2024)

Discovering quantum orders in mixed many-body systems is an ongoing issue. Very recently, the notion of an intrinsic mixed state topologically-ordered (IMTO) state was proposed. As a concrete example, we observe the emergence of IMTO by studying the toric code system under stochastic maximal decoherence by ZX-diagonal type projective measurement without monitoring. We study how the toric code state changes to an IMTO state at the level of the averaged quantum trajectories. This phase transition is understood from the viewpoint of spontaneous symmetry breaking (SSB) of 1-form weak symmetry, that is, the IMTO is characterized by the symmetry restoration from the SSB, which comes from the proliferation of anyons. To understand the emergent IMTO, order and disorder parameters of 1-form symmetry are numerically studied by stabilizer simulation. The present study clarifies the existence of two kinds of fermionic anyons, and also the obtained critical exponents indicate strong relation between IMTO and percolation.

Introduction.— Quantum devices such as quantum computers and quantum memory are significantly affected by quantum noise from external environment [1–5]. However, under noises, an intermediate scale quantum device and computer [6, 7] are expected to give some great ability beyond the ability of the classical ones [2]. Topologically ordered state [8–10], which is one of the non-trivial states of matter found first in condensed matter physics, gives a basic platform for topological quantum computations [11] or quantum memories [12]. Topological order has been already realized in experimental quantum systems [13–15]. Decoherence and noise from environment are inevitable and change quantum states into undesired ones. However, decoherence can lead to rich physical phenomena, leading to an unconventional quantum state of matter beyond the pure state. In particular, decoherence can create some unconventional topologically-ordered mixed states in quantum many-body systems. Recently, as an intriguing development, the notion of intrinsic mixed state topological order (IMTO) was proposed, i.e., the mixed state possesses some topological order with no counterparts in any pure states [16–19]. Interestingly, the IMTO can be distinguished or classified from the aspects of higher-form symmetries [20, 21] and their strong and/or weak spontaneous symmetry breaking (SSB). While the detailed notion of it has been discussed and its theoretical concept [16, 17, 22–28] is being developed, there are only a few concrete examples of emergent IMTO states studied by the numerical methods. We fill this gap in this letter.

We shall give a detailed study on the emergent IMTO under a stochastic ZX-type decoherence from the two-dimensional (2D) toric code (TC) stabilizer state, the system of which can be efficiently simulated in the stabilizer formalism. Further, we numerically investigate the critical properties of the phase transition as increasing the spatial rate of the decoherence, by observing density matrix trajectories [29] created through the large-scale stabilizer simulation [30, 31]. This phase transition is understood as a restoration from SSB of 1-form weak symmetries, that is, the IMTO is understood as a *disordered*

phase with respect to the 1-form weak symmetries, whereas the parent TC state is a strong-to-trivial SSB state. As a result of the phase transition, the content of relevant anyons is drastically changed, and anyon proliferation by the decoherence can be clearly understood from the perspective of the 1-form symmetries. The numerical simulation corroborates our consideration on the IMTO, and furthermore, it indicates that the transition to the IMTO is understood as a ‘percolation of decoherence’, supported by scaling analysis.

Toric code system under ZX-decoherence.— We consider the 2D TC system resided on torus. The system is shown in Fig. 1(a), where we introduce a lattice composed of $L_x \times L_y$ plaquettes (q -lattice) and $L_x \times L_y$ vertices (v -lattice) on the torus. Physical qubits reside on links of the v -lattice and then, the total number of qubit is $L \equiv 2L_x L_y$. We represent links by $\{\ell\}$, and we also use the link vector ℓ to the link number, that is, ℓ takes $\ell = 0, 1, 2, \dots, 2L_x L_y - 1$.

The initial state is set by the following stabilizer generators [32], $S_{\text{int}} = \{A_v | v \in \text{all vertex but } v_0\} + \{B_q | q \in \text{all plaquette but } q_0\}$. This state is the maximally-mixed ground state with the four-fold degeneracy of the TC on torus [12]. A_v and B_q are the star and plaquette operators; $A_v = \prod_{\ell_v \in v} X_{\ell_v}$ and $B_q = \prod_{\ell_q \in q} Z_{\ell_q}$, with $\ell_v \in v$ standing for links emanating from vertex v , and $\ell_q \in q$ for links composing plaquette q .

For later calculations, we add the typical logical operator into the set of the stabilizer generator as $\{S_{X-\text{lg}}\} = \prod_{\ell \in \gamma_{x(y)}} X_{\ell}$ where $\gamma_{x(y)}$ is $x(y)$ -directed non-contractible loop (the generator of 1-form electric Z_2 symmetry (‘t Hooft loop)) on the q -lattice. The stabilizer state (pure state) $S_{\text{int}} + S_{X-\text{lg}}$ is a TC state. We denote the density matrix by ρ_{TC} .

For the 2D system, we consider the channel of a local maximal ZX-coherence given by $\mathcal{E}_{\ell}^{\text{ZX}}[\rho] = \sum_{\beta_{\ell} = \pm 1} P_{\beta_{\ell}}^{\text{ZX}} \rho P_{\beta_{\ell}}^{\text{ZX}\dagger} = \frac{1}{2}\rho + \frac{1}{2}Z_{\ell} X_{\ell+\vec{\delta}} \rho Z_{\ell} X_{\ell+\vec{\delta}}$, where ρ is a state (density matrix), $\vec{\delta} = (1/2, -1/2)$ and β_i is a measurement outcome taking the value ± 1 . This decoherence corresponds to the projective measurement by $Z_{\ell} X_{\ell+\vec{\delta}}$ without

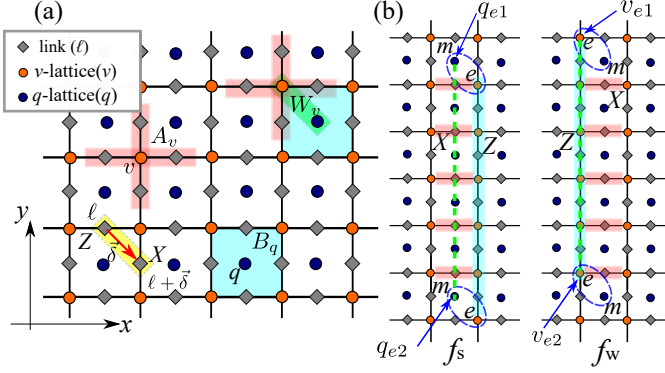


FIG. 1. (a) Schematic of toric code system. The red arrow is shift vector $\vec{\delta}$ used for definition of ZX and XZ operators. (b) The endpoints of open strings $\prod X_\ell Z_{\ell+\vec{\delta}}$ and $\prod Z_\ell X_{\ell+\vec{\delta}}$ create f_s and f_w -anyons, respectively, both of which are a fusion of e and m -anyons. Note that locations of e and m -anyons are different in f_s and f_w -anyons, that is, there are two kinds of f -anyons.

monitoring as shown in Fig. 1(a). The operation $Z_\ell X_{\ell+\vec{\delta}}$ also creates a pair of f -anyons (dyon) on the TC state as we explain later on [33].

Let us first consider a maximal ZX-decohered state, that is, for all links, the ZX-decoherence channel is applied as $\mathcal{E}^{all}[\rho] = \prod_{\ell=0}^{L-1} \mathcal{E}_\ell^{ZX}[\rho]$. Then, the obtained state is $\rho_f \equiv \mathcal{E}^{all}[\rho_{TC}]$. The state ρ_f is readily described by the stabilizer formalism as $\rho_f \propto \prod_{v=0}^{L_x L_y - 2} \frac{1+W_v}{2}$, where $W_v = A_v B_{v+\vec{\delta}}$ as shown in Fig. 1(a).

In order to understand the mixed state ρ_f , we introduce two kinds of 1-form symmetry, symmetry operators of which are defined as follows $W_{\gamma_c}^{ZX} \equiv \prod_{\ell \in \gamma_c} Z_\ell X_{\ell+\vec{\delta}}$ and $W_{\gamma_c}^{XZ} \equiv \prod_{\ell \in \gamma_c} X_\ell Z_{\ell+\vec{\delta}}$ with a contractible loop γ_c on the links of the v lattice. It is easily seen that the operator $W_{\gamma_c}^{ZX}$ is a product of consecutive Kraus operators, $\{Z_\ell X_{\ell+\vec{\delta}}\}$, and satisfies the 1-form weak-symmetry condition [34] [see the definition of weak and strong symmetries in [35]], $W_{\gamma_c}^{ZX} \rho_f W_{\gamma_c}^{ZX} = \rho_f$, although it *does not* commute some of Kraus operators. On the other hand, the operator $W_{\gamma_c}^{XZ}$ commutes all of the Kraus operators and $W_{\gamma_c}^{ZX}$, and satisfies the 1-form strong-symmetry condition [34], $W_{\gamma_c}^{XZ} \rho_f = \rho_f W_{\gamma_c}^{XZ} = \rho_f$. By employing open string \mathcal{C} instead of the close loop γ_c for the above operators, corresponding anyons emerge at the endpoints of \mathcal{C} as shown in Fig. 1(b). We call them f_w and f_s , respectively. We remark that both the anyons are obtained by the fusion of e -anyon and m -anyons but their geometric location is different in f_w and f_s . This point has been overlooked so far and plays an important role in understanding ρ_f . It is not so difficult to show $W_{\mathcal{C}}^{ZX} \rho_f W_{\mathcal{C}}^{ZX} = \rho_f$, which implies emergence of f_w -anyon proliferation in ρ_f [16, 17]. On the other hand, the operator $W_{\mathcal{C}}^{XZ}$ does not commute with the stabilizer W_v at endpoints, and therefore, f_s -anyon is a detectable anyon behaving as a stable excited state, whereas f_w -anyon

is an undetectable anyon to proliferate [36]. The states ρ_{TC} and ρ_f are classified from the viewpoint of SSB/non-SSB of the 1-form symmetries proposed recently [37]. The 1-form symmetry aspect is discussed in detail in supplemental material (SM) [35], and it is emphasized there that the order and disorder parameters of the 1-form symmetries give us useful measures for the phase transition from the TC state (topological SSB state) to the IMTO state.

Target physical quantities.— To understand the effect of the ZX-decoherence and detect the IMTO, we focus on analyzing the following physical quantities.

Specific behavior of entanglement negativity: We firstly focus on the entanglement negativity for a contractible closed subsystem given as $N_A \equiv \log_2 |\rho^{\Gamma_A}|_1$ [38, 39], where $|\cdot|_1$ is the trace norm and Γ_A is a partial transpose for A-subsystem. The negativity can reveal a transition of states under decoherence by quantifying quantum correlations in mixed states [40–42]. The practical method of numerical calculation in the stabilizer formalism is explained in the SM [35]. As the A-subsystem, we use a rectangular subsystem on the v -lattice of size $\ell_x \times \ell_y$, with $\ell_x = 2k_A$ and $\ell_y = 2(k_A \in \mathbb{N}^0)$ as in Fig. 2(b). Then as in Ref. [16], a specific behavior of the negativity is expected for the maximal ZX-decoherence limit ρ_f , i.e., the subsystem size scaling of the negativity given by $N_A^f(k_A) = \frac{N_P}{2} - \frac{1}{2}$ with $N_P = 6(k_A + 1)$. We shall observe whether such a scaling holds in the ZX-decohered system later. Furthermore, as the negativity is a measure of the long-range entanglement, its comparison with the behavior of the logical operator is interesting. We shall discuss this point after showing the numerical results.

Order and disorder parameters for 1-form weak SSB: To characterize the IMTO, we shall make use of a 1-form symmetry picture and its SSB, the generator of which is given by $W_{\gamma_c}^{ZX}$, here we only consider a contractible loop γ_c on the v -lattice as before.

The system density matrix ρ starting with ρ_{TC} keeps the 1-form weak symmetry $W_{\gamma_c}^{ZX} \rho W_{\gamma_c}^{ZX\dagger} = \rho$ [34, 43] through the ZX-channels \mathcal{E}_ℓ^{ZX} , since the symmetry generator $W_{\gamma_c}^{ZX}$ anti-commutes with some of Kraus operators but commutes with all of the stabilizers [35]. Based on this symmetry, its SSB can be detected by the following two observables.

As suggested by Ref. [37], the order parameter of the 1-form weak SSB is given by $C^I(\rho, \gamma'_c) \equiv \text{Tr}[\rho W_{\gamma'_c}^Z] / \text{Tr}[\rho^2]$, where γ'_c is a contractible loop on the v -lattice, and $W_{\gamma'_c}^Z \equiv \prod_{\ell \in \gamma'_c} Z_\ell$ is a Wilson loop, one of conjugate operators to $W_{\gamma_c}^{ZX}$, coming from the fact that e -anyon and f_w -anyon have nontrivial braiding relation. The finite value of $C^I(\rho, \gamma'_c)$ for a large loop γ'_c means the 1-form weak SSB. In fact, the initial state $C^I(\rho_{TC}, \gamma'_c) = 1$. For later numerics, we practically calculate the average sum of $C^I(\rho, \gamma'_c)$ for different typical square loop $\gamma'_c(k)$ (the side of the length is $\ell_x = \ell_y = k$), and define $\chi^I[\rho] \equiv \frac{1}{N_\ell} \sum_{k=1}^{N_\ell} C^I(\rho, \gamma'_c(k))$ with $N_\ell = \min\{L_x - 2, L_y - 2\}$.

The disorder parameter is given by $C^{\text{II}}(\rho, (v_{e1}, v_{e2})) \equiv$

$\text{Tr}[\rho W^{ZX}(v_{e1}, v_{e2}) \rho W^{ZX}(v_{e1}, v_{e2})] / \text{Tr}[\rho^2]$, where $W^{ZX}(v_{e1}, v_{e2})$ is an open string operator W_C^{ZX} for \mathcal{C} of endpoints v_{e1} and v_{e2} , as shown in Fig. 1(b). The observable $C^{\text{II}}(\rho, (v_{e1}, v_{e2}))$ is an extension of the Rényi-2 correlator used for study on weak-symmetry SSB in ‘spin’ systems [22–25, 37]. For the initial state $C^{\text{II}}(\rho_{\text{TC}}, (v_{e1}, v_{e2})) = 0$, which means that TC state is strong-to-trivial SSB. We shall calculate this quantity under the ZX decoherence channel to observe a transition to the IMTO. For later numerics, we practically calculate the susceptibility defined by $\chi^{\text{II}}(\rho) \equiv \frac{1}{L_x(L_y-3)} \sum_{i_x=0}^{L_x-1} \sum_{\ell=1}^{L_y-3} C^{\text{II}}(\rho, ((i_x, 0), (i_x, \ell)))$ for a state ρ , where $(i_x, 0)$ and (i_x, ℓ) are the locations of e -anyons residing on the endpoints of the open string.

Stochastic ZX-decoherence-only stabilizer channel and trajectory ensemble.— We consider a stabilizer channel consisting of solely ZX-decoherences, where the local ZX-decoherence at diagonal links \mathcal{E}_ℓ is applied with a probability r for all links ℓ , that is, we consider a single-layer decoherence. Such local decoherence is numerically tractable in the algorithm even for large system sizes [42], as explained in [35]. In the system under the decoherence, we record locations of the occurrence of decoherence but no other information of the channel. The system with this protocol exhibits a single trajectory of the state labeled by s , described as $\rho_D^s = \mathcal{E}_{\ell_0}^{ZX} \circ \mathcal{E}_{\ell_1}^{ZX} \circ \dots \circ \mathcal{E}_{\ell_{N_D}}^{ZX} [\rho_0]$, where ρ_D^s is the final mixed state after the single-layer decoherence, ρ_0 is an initial state, $\mathcal{E}_{\ell_k}^{ZX}$ is the ZX decoherence at a position ℓ_k , and N_D is the number of $\mathcal{E}_{\ell_k}^{ZX}$ performed with the probability r ($N_D \sim r \times [\text{total number of site}]$). Similar setups were used in Refs. [25, 29, 42, 44, 45].

By using these trajectory samples $\{\rho_D^s\}$, we obtain the ensemble average of the physical quantities denoted as $Q(\rho_D^s)$ introduced in the previous sections. This quantity is given by the non-linear form of the density matrix [46], denoted by $\mathbb{E}[Q(\rho_D^s)]$, where $\mathbb{E}[\cdot]$ means averaging over the samples of the trajectory density matrix ρ_D^s . We shall show that the IMTO state appears in the level of quantum trajectory ensemble.

Numerical results for averaged physical quantities.— We shall show the numerical results in the stochastic ZX-decoherence circuit.

Averaged entanglement negativity: We plot subsystem-size dependence of $\mathbb{E}[N_A(k_A)]$ on k_A for various r 's with fixing the system size as $(L_x, L_y) = (20, 6)$. As shown in Fig. 2(a), the k_A linear scaling line of $\mathbb{E}[N_A]$ rapidly approaches the scaling line of the maximal ZX-decoherence state ρ_f [16]. This rapid approach is a signature of the phase transition to the IMTO having the same long-range entanglement (LRE) with ρ_f . Location of the critical point is elucidated by observing the difference between the analytical calculation N_A^f and numerically-obtained one $\mathbb{E}[N_A(k_A)]$ defined as $\Delta_0 N_A(r) \equiv \sum_{k_A=1}^{(L_x-2)/2} (\mathbb{E}[N_A(k_A, r)] - N_A^f)^2$. The data is displayed in Fig. 2(c), which shows $\Delta_0 N_A(r = 0.5) \approx 0$ for the various system sizes, and we estimate the critical point as $r_c = 0.5$.

The system-size independent term in N_A^f indicates the existence of the LRE even for $r > r_c$. We also investigated the

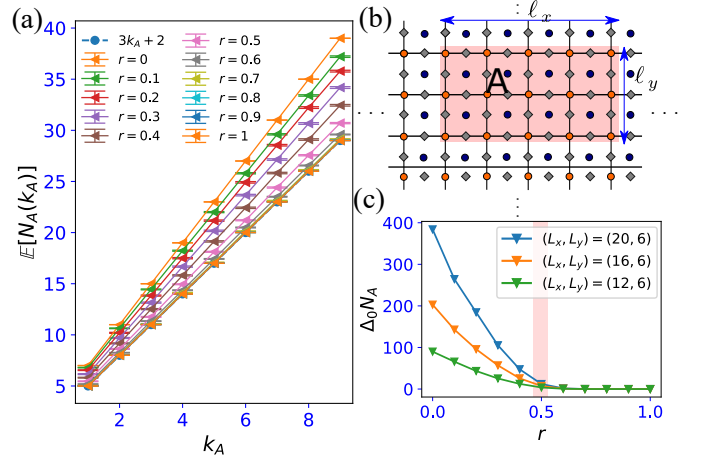


FIG. 2. (a) $\mathbb{E}[N_A(k_A, r)]$ for different r 's. (b) The subsystem partition for N_A . The rectangle edges are $l_x = 2k_A$ and $l_y = 2$ with $k_A \in \mathbb{N}^0$ (c) The behavior of $\Delta_0 N_A(r, L_x)$. The number of sample trajectories is $\mathcal{O}(10^2)$.

behavior of the logical qubit, i.e., the annihilation probability of the logical operators of the TC under the ZX-decoherence, and found that it disappears at $r \sim 0.5$ (see [35]). As suggested in [16], this is a typical behavior of the IMTO, and the origin of the LRE is to be clarified in a later research.

Averaged 1-form weak SSB restoring transition: Let us study how the SSB properties of the system change under the decoherence. For the order parameter $C^{\text{I}}(\rho, \gamma'_c)$, the initial state ρ_{TC} has $C^{\text{I}}(\rho_{\text{TC}}, \gamma'_c) = 1$ since the closed loop $W_{\gamma'_c}^Z$ is given by a product of B_p 's and is an element of the stabilizer group of the TC. This fact means that the state ρ_{TC} is a 1-form weak SSB state [47]. By the decoherence \mathcal{E}_ℓ^{ZX} with Kraus operators, some of which anti-commute with the operator $W_{\gamma'_c}^Z$, $W_{\gamma'_c}^Z$ tends to disappear in the stabilizer group as r is getting large, inducing $C^{\text{I}}(\rho_{\text{TC}}, \gamma'_c) \rightarrow 0$. [The numerical calculation method of C^{I} is explained in [35]].

For the disorder parameter $C^{\text{II}}(\rho, (v_{e1}, v_{e2}))$, certain A_v and B_p stabilizers of ρ_{TC} anti-commute with both endpoints of the open string $W^{ZX}(v_{e1}, v_{e2})$, resulting in $C^{\text{II}}(\rho_{\text{TC}}, (v_{e1}, v_{e2})) = 0$. [See the calculation of the Rényi-2 correlator [35].] As increasing r , the operator W_v proliferates and becomes a stabilizer generator of the mixed state. Then, the open string $W^{ZX}(v_{e1}, v_{e2})$ tends to commute with the set of the stabilizer generators of the decohered state instead of A_v and B_p . In the limit $r = 1$, the state ρ_f commutes with any open string $W^{ZX}(v_{e1}, v_{e2})$, leading to $C^{\text{II}}(\rho_f, (v_{e1}, v_{e2})) = 1$. Thus, the stochastic circuit tends to increase the value of $C^{\text{II}}(\rho, (v_{e1}, v_{e2}))$ and the decohered state turns into a state restoring the 1-form weak symmetry. Note that since the open string operator $W^{ZX}(v_{e1}, v_{e2})$ creates f_w -anyon at the endpoints, the finite value of $C^{\text{II}}(\rho_f, (v_{e1}, v_{e2}))$ means that the f_w -anyons proliferate in the state through the decoherence.

Based on the above observation, let us numerically study

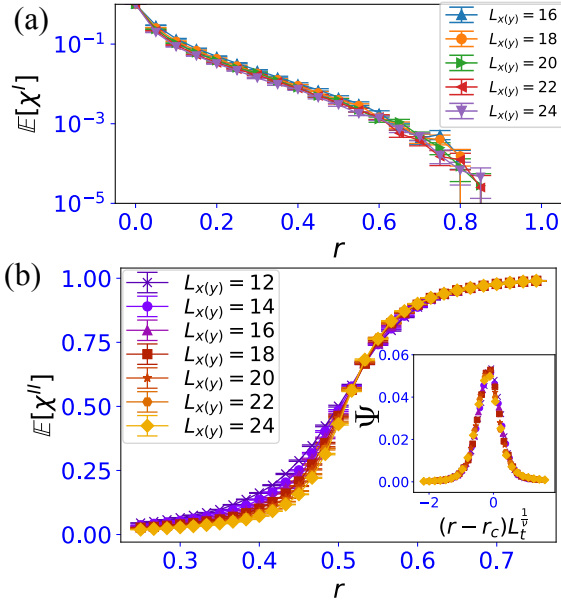


FIG. 3. (a) The behavior of $\mathbb{E}[\chi^I]$. (b) The behavior of $\mathbb{E}[\chi^{II}]$. Inset: the scaling collapse for the rescaled variance F . For each data, we averaged over $\mathcal{O}(10^3)$ samples.

the average of χ^I and χ^{II} , $\mathbb{E}[\chi^I(\rho_s, r)]$ and $\mathbb{E}[\chi^{II}(\rho_s, r)]$, to verify the behavior of the order and disorder parameters.

As shown in Fig. 3(a), $\mathbb{E}[\chi^I(\rho_s, r)]$ starts from the state ρ_{TC} with $\chi^I = 1$ and decreases as increasing r , indicating the vanishing of the weak SSB order for the 1-form weak symmetry of the generator $W_{\gamma_c}^{ZX}$. However, $\mathbb{E}[\chi^I(\rho_s, r)]$ does not exhibit any particular behaviors in the vicinity of the expected transition point $r \sim 0.5$. This might be not so surprising as the genuine expectation value of the Wilson loop, $\text{Tr}(W_{\gamma_c}^Z \rho)$, does not show any indication of the decoherence transition [48]. Therefore, study using disorder parameter is quite useful for observing the decoherent transition.

As explained in the above, the quantity $\mathbb{E}[\chi^{II}(\rho_s, r)]$ is more suitable for detecting the phase transition of the mixed state as shown in [25]. The numerical data of $\mathbb{E}[\chi^{II}(\rho_s, r)]$ is shown in Fig. 3(b). We find that the value of $\mathbb{E}[\chi^{II}(\rho_s, r)]$ exhibits a sudden change around $r = 0.5$, indicating the disordered state for the 1-form weak symmetry of the generator $W_{\gamma_c}^{ZX}$ appears as increasing r . We find that combining this behavior with the result of N_A in Figs. 2(a) and (c), the transition from the TC state to the IMTO state takes place at $r \simeq 0.5$.

Furthermore, through the variance σ obtained from many samples of the quantity $(L_x(L_y - 3)\chi^{II}(\rho_s, r))$ for various system sizes, we identify the critical probability of the phase transition r_c and study its criticality. Here, we employ a rescaled variance $F \equiv \sigma/(L_x(L_y - 3))$ and the finite-size scaling ansatz given such as $F \equiv L_t^{\zeta} \Psi((r - r_c)L_t^{\frac{1}{\nu}})$, where the system typical length L_t , and ζ and ν are critical exponents. [The detailed behavior of the rescaled χ^{II} and rescaled

variance F are shown in [35].] In particular, we are interested in the exponent ν (correlation length critical exponent). We set $L_t = L_x$ and employ pyfssa package [49, 50]. The best scaling collapse data in our numerics is shown in the inset of Fig. 3(b). We here estimate $r_c = 0.528 \pm 0.007$, $\nu = 1.36 \pm 0.47$ and $\zeta = 2.65 \pm 0.37$. We find that the exponent ν is very close to that of the 2D percolation $4/3$ [51]. Thus, we expect that the phase transition found here relates to 2D classical percolation. In fact in the previous paper [25], we discussed how the decoherent transition is related to the percolation from the viewpoint of stabilizer channel, and that observation is applied to the present ‘gauge system’ rather straightforwardly.

Discussion and conclusion.— In this letter, we gave a concrete demonstration of the emergence of the IMTO from the genuine topological state (the TC state) in the stochastic ZX-decoherence channel. In particular, we found the phase transition that is understood as the restoration of the 1-form weak symmetry and anyon proliferation, and verified the expectation that its phase transition is closely related to the 2D percolation by estimating the critical exponents. Finally, we comment that studying the relation to subsystem code [17, 36, 52–54] is an interesting future direction.

Acknowledgements.— This work is supported by JSPS KAKENHI: JP23K13026(Y.K.) and JP23KJ0360(T.O.).

* A professor emeritus

- [1] C. W. Gardiner and P. Zoller, *Quantum Noise*, 2nd ed., edited by H. Haken (Springer, 2000).
- [2] J. Preskill, Quantum computing in the nisq era and beyond, *Quantum* **2**, 79 (2018).
- [3] E. Dennis, A. Kitaev, A. Landahl, and J. Preskill, Topological quantum memory, *Journal of Mathematical Physics* **43**, 4452–4505 (2002).
- [4] C. Wang, J. Harrington, and J. Preskill, Confinement-higgs transition in a disordered gauge theory and the accuracy threshold for quantum memory, *Annals of Physics* **303**, 31–58 (2003).
- [5] T. Ohno, G. Arakawa, I. Ichinose, and T. Matsui, Phase structure of the random-plaquette z2 gauge model: accuracy threshold for a toric quantum memory, *Nuclear Physics B* **697**, 462 (2004).
- [6] S. Ebadi, T. T. Wang, H. Levine, A. Keesling, G. Semeghini, A. Omran, D. Bluvstein, R. Samajdar, H. Pichler, W. W. Ho, S. Choi, S. Sachdev, M. Greiner, V. Vladan, and M. D. Lukin, Quantum phases of matter on a 256-atom programmable quantum simulator, *Nature* **595**, 227 (2021).
- [7] D. Bluvstein, S. J. Evered, A. A. Geim, S. H. Li, H. Zhou, T. Manovitz, S. Ebadi, M. Cain, M. Kalinowski, D. Hangleiter, J. P. Bonilla Ataides, N. Maskara, I. Cong, X. Gao, P. Sales Rodriguez, T. Karolyshyn, G. Semeghini, M. J. Gullans, M. Greiner, V. Vladan, and M. D. Lukin, Logical quantum processor based on reconfigurable atom arrays, *Nature* **626**, 58 (2024).
- [8] X.-G. Wen, *Quantum field theory of many-body systems: From the origin of sound to an origin of light and electrons* (2007).
- [9] X.-G. Wen, Colloquium: Zoo of quantum-topological phases of matter, *Rev. Mod. Phys.* **89**, 041004 (2017).

- [10] B. Zeng, X. Chen, D.-L. Zhou, and X.-G. Wen, [Quantum information meets quantum matter – from quantum entanglement to topological phase in many-body systems](#) (2018), [arXiv:1508.02595 \[cond-mat.str-el\]](#).
- [11] C. Nayak, S. H. Simon, A. Stern, M. Freedman, and S. Das Sarma, Non-abelian anyons and topological quantum computation, *Rev. Mod. Phys.* **80**, 1083 (2008).
- [12] A. Kitaev, Fault-tolerant quantum computation by anyons, *Annals of Physics* **303**, 2–30 (2003).
- [13] K. J. Satzinger, Y.-J. Liu, A. Smith, C. Knapp, M. Newman, C. Jones, Z. Chen, C. Quintana, X. Mi, A. Dunsworth, C. Gidney, I. Aleiner, F. Arute, K. Arya, J. Atalaya, R. Babbush, J. C. Bardin, R. Barends, J. Basso, A. Bengtsson, A. Bilmes, M. Broughton, B. B. Buckley, D. A. Buell, B. Burkett, N. Bushnell, B. Chiaro, R. Collins, W. Courtney, S. Demura, A. R. Derk, D. Eppens, C. Erickson, L. Faoro, E. Farhi, A. G. Fowler, B. Foxen, M. Giustina, A. Greene, J. A. Gross, M. P. Harrigan, S. D. Harrington, J. Hilton, S. Hong, T. Huang, W. J. Huggins, L. B. Ioffe, S. V. Isakov, E. Jeffrey, Z. Jiang, D. Kafri, K. Kechedzhi, T. Khattar, S. Kim, P. V. Klimov, A. N. Korotkov, F. Kostritsa, D. Landhuis, P. Laptev, A. Locharla, E. Lucero, O. Martin, J. R. McClean, M. McEwen, K. C. Miao, M. Mohseni, S. Montazeri, W. Mruczkiewicz, J. Mutus, O. Naaman, M. Neeley, C. Neill, M. Y. Niu, T. E. O’Brien, A. Opremcak, B. Pató, A. Petukhov, N. C. Rubin, D. Sank, V. Shvarts, D. Strain, M. Szalay, B. Villalonga, T. C. White, Z. Yao, P. Yeh, J. Yoo, A. Zalcman, H. Neven, S. Boixo, A. Megrant, Y. Chen, J. Kelly, V. Smelyanskiy, A. Kitaev, M. Knap, F. Pollmann, and P. Roushan, Realizing topologically ordered states on a quantum processor, *Science* **374**, 1237–1241 (2021).
- [14] R. Acharya, I. Aleiner, R. Allen, T. I. Andersen, M. Ansmann, F. Arute, K. Arya, A. Asfaw, J. Atalaya, R. Babbush, D. Bacon, J. C. Bardin, J. Basso, A. Bengtsson, S. Boixo, G. Bortoli, A. Bourassa, J. Bovaird, L. Brill, M. Broughton, B. B. Buckley, D. A. Buell, T. Burger, B. Burkett, N. Bushnell, Y. Chen, Z. Chen, B. Chiaro, J. Cogan, R. Collins, P. Conner, W. Courtney, A. L. Crook, B. Curtin, D. M. Debroy, A. D. T. Barba, S. Demura, A. Dunsworth, D. Eppens, C. Erickson, L. Faoro, E. Farhi, R. Fatemi, L. F. Burgos, E. Forati, A. G. Fowler, B. Foxen, W. Giang, C. Gidney, D. Gilboa, M. Giustina, A. G. Dau, J. A. Gross, S. Habegger, M. C. Hamilton, M. P. Harrigan, S. D. Harrington, O. Higgott, J. Hilton, M. Hoffmann, S. Hong, T. Huang, A. Huff, W. J. Huggins, L. B. Ioffe, S. V. Isakov, J. Iveland, E. Jeffrey, Z. Jiang, C. Jones, P. Juhas, D. Kafri, K. Kechedzhi, J. Kelly, T. Khattar, M. Khezri, M. Kieferová, S. Kim, A. Kitaev, P. V. Klimov, A. R. Klots, A. N. Korotkov, F. Kostritsa, J. M. Kreikebaum, D. Landhuis, P. Laptev, K.-M. Lau, L. Laws, J. Lee, K. Lee, B. J. Lester, A. Lill, W. Liu, A. Locharla, E. Lucero, F. D. Malone, J. Marshall, O. Martin, J. R. McClean, T. Mccourt, M. McEwen, A. Megrant, B. M. Costa, X. Mi, K. C. Miao, M. Mohseni, S. Montazeri, A. Morvan, E. Mount, W. Mruczkiewicz, O. Naaman, M. Neeley, C. Neill, A. Nersisyan, H. Neven, M. Newman, J. H. Ng, A. Nguyen, M. Nguyen, M. Y. Niu, T. E. O’Brien, A. Opremcak, J. Platt, A. Petukhov, R. Potter, L. P. Pryadko, C. Quintana, P. Roushan, N. C. Rubin, N. Saei, D. Sank, K. Sankaragomathi, K. J. Satzinger, H. F. Schurkus, C. Schuster, M. J. Shearn, A. Shorter, V. Shvarts, J. Skrzynny, V. Smelyanskiy, W. C. Smith, G. Sterling, D. Strain, M. Szalay, A. Torres, G. Vidal, B. Villalonga, C. V. Heidweiller, T. White, C. Xing, Z. J. Yao, P. Yeh, J. Yoo, G. Young, A. Zalcman, Y. Zhang, and N. Zhu, [Suppressing quantum errors by scaling a surface code logical qubit](#) (2022), [arXiv:2207.06431 \[quant-ph\]](#).
- [15] Y. Zhao, Y. Ye, H.-L. Huang, Y. Zhang, D. Wu, H. Guan, Q. Zhu, Z. Wei, T. He, S. Cao, F. Chen, T.-H. Chung, H. Deng, D. Fan, M. Gong, C. Guo, S. Guo, L. Han, N. Li, S. Li, Y. Li, F. Liang, J. Lin, H. Qian, H. Rong, H. Su, L. Sun, S. Wang, Y. Wu, Y. Xu, C. Ying, J. Yu, C. Zha, K. Zhang, Y.-H. Huo, C.-Y. Lu, C.-Z. Peng, X. Zhu, and J.-W. Pan, Realization of an error-correcting surface code with superconducting qubits, *Phys. Rev. Lett.* **129**, 030501 (2022).
- [16] Z. Wang, Z. Wu, and Z. Wang, [Intrinsic mixed-state quantum topological order](#) (2024), [arXiv:2307.13758 \[quant-ph\]](#).
- [17] R. Sohal and A. Prem, [A noisy approach to intrinsically mixed-state topological order](#) (2024), [arXiv:2403.13879 \[cond-mat.str-el\]](#).
- [18] S. Sang, Y. Zou, and T. H. Hsieh, Mixed-state quantum phases: Renormalization and quantum error correction, *Phys. Rev. X* **14**, 031044 (2024).
- [19] Y.-H. Chen and T. Grover, Unconventional topological mixed-state transition and critical phase induced by self-dual coherent errors, *Phys. Rev. B* **110**, 125152 (2024).
- [20] D. Gaiotto, A. Kapustin, N. Seiberg, and B. Willett, Generalized global symmetries, *Journal of High Energy Physics* **2015**, 172 (2015).
- [21] J. McGreevy, Generalized symmetries in condensed matter, *Annual Review of Condensed Matter Physics* **14**, 57–82 (2023).
- [22] J. Y. Lee, C.-M. Jian, and C. Xu, Quantum criticality under decoherence or weak measurement, *PRX Quantum* **4**, 030317 (2023).
- [23] L. A. Lessa, R. Ma, J.-H. Zhang, Z. Bi, M. Cheng, and C. Wang, [Strong-to-weak spontaneous symmetry breaking in mixed quantum states](#) (2024), [arXiv:2405.03639 \[quant-ph\]](#).
- [24] P. Sala, S. Gopalakrishnan, M. Oshikawa, and Y. You, [Spontaneous strong symmetry breaking in open systems: Purification perspective](#) (2024), [arXiv:2405.02402 \[quant-ph\]](#).
- [25] Y. Kuno, T. Orito, and I. Ichinose, Strong-to-weak symmetry breaking states in stochastic dephasing stabilizer circuits, *Phys. Rev. B* **110**, 094106 (2024).
- [26] Z. Liu, L. Chen, Y. Zhang, S. Zhou, and P. Zhang, [Diagnosing strong-to-weak symmetry breaking via wightman correlators](#) (2024), [arXiv:2410.09327 \[quant-ph\]](#).
- [27] Y. Guo and S. Yang, [Strong-to-weak spontaneous symmetry breaking meets average symmetry-protected topological order](#) (2024), [arXiv:2410.13734 \[cond-mat.str-el\]](#).
- [28] J. Shah, C. Fechisin, Y.-X. Wang, J. T. Iosue, J. D. Watson, Y.-Q. Wang, B. Ware, A. V. Gorshkov, and C.-J. Lin, [Instability of steady-state mixed-state symmetry-protected topological order to strong-to-weak spontaneous symmetry breaking](#) (2024), [arXiv:2410.12900 \[quant-ph\]](#).
- [29] M. J. Gullans and D. A. Huse, Dynamical purification phase transition induced by quantum measurements, *Phys. Rev. X* **10**, 041020 (2020).
- [30] D. Gottesman, [The heisenberg representation of quantum computers](#) (1998), [arXiv:quant-ph/9807006 \[quant-ph\]](#).
- [31] S. Aaronson and D. Gottesman, Improved simulation of stabilizer circuits, *Phys. Rev. A* **70**, 052328 (2004).
- [32] M. A. Nielsen and I. L. Chuang, [Quantum Computation and Quantum Information](#), 10th ed. (Cambridge University Press, USA, 2011).
- [33] G. Arakawa and I. Ichinose, Zn gauge theories on a lattice and quantum memory, *Annals of Physics* **311**, 152 (2004).
- [34] C. de Groot, A. Turzillo, and N. Schuch, Symmetry protected topological order in open quantum systems, *Quantum* **6**, 856 (2022).
- [35] See the supplemental material: A. Definition of strong and weak symmetry for density matrix, B. Symmetry aspects for the system, C. Numerical scheme, D. Annihilation probability

- of logical operator of toric code, and E. Rescaled χ^{II} and its rescaled variance.
- [36] T. D. Ellison, Y.-A. Chen, A. Dua, W. Shirley, N. Tanti-vasadakarn, and D. J. Williamson, Pauli topological subsystem codes from Abelian anyon theories, *Quantum* **7**, 1137 (2023).
- [37] C. Zhang, Y. Xu, J.-H. Zhang, C. Xu, Z. Bi, and Z.-X. Luo, Strong-to-weak spontaneous breaking of 1-form symmetry and intrinsically mixed topological order (2024), arXiv:2409.17530 [quant-ph].
- [38] A. Peres, Separability criterion for density matrices, *Phys. Rev. Lett.* **77**, 1413 (1996).
- [39] R. Horodecki, P. Horodecki, M. Horodecki, and K. Horodecki, Quantum entanglement, *Rev. Mod. Phys.* **81**, 865 (2009).
- [40] T.-C. Lu, T. H. Hsieh, and T. Grover, Detecting topological order at finite temperature using entanglement negativity, *Phys. Rev. Lett.* **125**, 116801 (2020).
- [41] S. Sang, Y. Li, T. Zhou, X. Chen, T. H. Hsieh, and M. P. Fisher, Entanglement negativity at measurement-induced criticality, *PRX Quantum* **2**, 030313 (2021).
- [42] Z. Weinstein, Y. Bao, and E. Altman, Measurement-induced power-law negativity in an open monitored quantum circuit, *Phys. Rev. Lett.* **129**, 080501 (2022).
- [43] R. Ma, J.-H. Zhang, Z. Bi, M. Cheng, and C. Wang, Topological phases with average symmetries: the decohered, the disordered, and the intrinsic (2024), arXiv:2305.16399 [cond-mat.str-el].
- [44] S. Liu, M.-R. Li, S.-X. Zhang, and S.-K. Jian, Entanglement structure and information protection in noisy hybrid quantum circuits, *Phys. Rev. Lett.* **132**, 240402 (2024).
- [45] S. Liu, M.-R. Li, S.-X. Zhang, S.-K. Jian, and H. Yao, Noise-induced phase transitions in hybrid quantum circuits, *Phys. Rev. B* **110**, 064323 (2024).
- [46] Physical quantities given by some linear form of the density matrix ρ becomes zero in the trajectory ensemble average.
- [47] Note that strictly the state ρ_{TC} is 1-form strong symmetric for 1-form symmetry $W_{\gamma_c}^{ZX}$ as $W_{\gamma_c}^{ZX}\rho_{TC}$. But, we needs to include the channel decoherence dynamics \mathcal{E}^{ZX} , which is not strong symmetric. Thus, we regard that ρ_{TC} is also weak symmetric.
- [48] Y. Bao, R. Fan, A. Vishwanath, and E. Altman, Mixed-state topological order and the errorfield double formulation of decoherence-induced transitions (2023), arXiv:2301.05687 [quant-ph].
- [49] O. Melchert, autoscale.py - a program for automatic finite-size scaling analyses: A user's guide (2009), arXiv:0910.5403 [physics.comp-ph].
- [50] A. Sorge, autoscale.py - a program for automatic finite-size scaling analyses: A user's guide (2015).
- [51] D. Stauffer and A. Aharony, *Introduction To Percolation Theory: Second Edition* (CRC Press, 2018).
- [52] D. Poulin, Stabilizer formalism for operator quantum error correction, *Phys. Rev. Lett.* **95**, 230504 (2005).
- [53] D. Bacon, Operator quantum error-correcting subsystems for self-correcting quantum memories, *Phys. Rev. A* **73**, 012340 (2006).
- [54] Y. Kuno and I. Ichinose, Interplay between lattice gauge theory and subsystem codes, *Phys. Rev. B* **108**, 045150 (2023).
- [55] B. Shi, X. Dai, and Y.-M. Lu, Entanglement negativity at the critical point of measurement-driven transition (2021), arXiv:2012.00040 [cond-mat.stat-mech].
- [56] S. Sharma, X. Turkeshi, R. Fazio, and M. Dalmonte, Measurement-induced criticality in extended and long-range unitary circuits, *SciPost Phys. Core* **5**, 023 (2022).
- [57] Y. Kuno, T. Orito, and I. Ichinose, Phase transition and evidence of fast-scrambling phase in measurement-only quantum circuits, *Phys. Rev. B* **108**, 094104 (2023).
- [58] T. Botzung, M. Buchhold, S. Diehl, and M. Müller, Robustness and measurement-induced percolation of the surface code (2023), arXiv:2311.14338 [quant-ph].

SUPPLEMENTAL MATERIAL:

A. Definition of strong and weak symmetry for density matrix

We give a brief summery for the definition of the strong and weak symmetries for a density matrix.

In general, a density matrix (mixed state) can have two types of symmetries: strong and weak symmetries. The condition of the strong symmetry to a state ρ is given as [34]

$$U_g \rho = e^{i\theta} \rho,$$

where ρ is a state (pure or mixed) and U_g is a symmetry operation of an element g of a symmetry group G and θ is a certain global phase factor.

Next, the weak symmetry is characterized by

$$U_g \rho U_g^\dagger = \rho.$$

This condition is called the average or weak symmetry [43], as the symmetry is satisfied in the ensemble in general. Note that if a state ρ has a strong symmetry, the state is also weak symmetric with respect to that symmetry.

These notions are also applicable to quantum channels $\mathcal{E}(\rho)$. Here, we consider the operator-sum representation of the channel [32],

$$\mathcal{E}(\rho) = \sum_{\ell=0}^{N-1} K_\ell \rho K_\ell^\dagger,$$

where K_ℓ 's are Kraus operators satisfying $\sum_{\ell=0}^{N-1} K_\ell^\dagger K_\ell = I$. The channel \mathcal{E} changes the input state ρ , and it includes non-unitary transformations such as decoherence and quantum measurements.

For the channel \mathcal{E} , the strong symmetry condition on the channel for a symmetry G is represented as [34]

$$K_\ell U_g = e^{i\theta} U_g K_\ell$$

for $\forall \ell$ and $g \in G$, where θ is a single phase. On the other hand, weak symmetry condition on the channel for a symmetry G is given as

$$U_g \left[\sum_{\ell} K_\ell \rho K_\ell^\dagger \right] U_g^\dagger = \mathcal{E}(\rho).$$

All Kraus operators $\{K_\ell\}$ do not necessarily commute with U_g .

B. Symmetry aspects for the system

We can introduce various types of 1-form symmetries by considering loop Pauli string operators [16, 17]. In what follows, we discuss some kinds of symmetries regarded as weak or strong 1-form symmetries, which play an important role for the classification of topological order (TO), and then consider their SSB [37] for the typical pure and mixed states, ρ_{TC} and ρ_f in the main text.

In the toric code (TC) state, ρ_{TC} , there are two 1-form strong symmetries, which are often represented by the Wilson and 't Hooft loop operators, and the anyon content is given as $\{1, e, m, f\}$, where $e(m)$ referees to electric (magnetic) anyon, as well as their fusion $f = (e \times m)$. In the IMTO state, ρ_f , on the other hand, the structure of the 1-form symmetry is slightly complicated as the state emerges through the decoherence by Kraus operators, some of which are non-commutative. As a result, loop operators of the 1-form symmetries are a product of composite operators as we clarify in this section.

1. Contractible loop W^{ZX} type of 1-form symmetry: The first 1-form symmetry in ρ_f is given by a product of Kraus operators along an arbitrary contractible loop on v -lattice γ_c ; $W_{\gamma_c}^{ZX} = \prod_{\ell \in \gamma_c} Z_\ell X_{\ell+\delta}$. It is verified that $W_{\gamma_c}^{ZX}$ anti-commutes with some of Kraus operators but commutes with all of the stabilizers. The channel \mathcal{E}^{ZX} satisfies the condition of 1-form weak symmetry [34] since for a local channel for any link ℓ , $\mathcal{E}_\ell^{ZX}(\rho) = \frac{1}{2}\rho + \frac{1}{2}Z_\ell X_{\ell+\delta}\rho Z_\ell X_{\ell+\delta}$, $W_{\gamma_c}^{ZX}\mathcal{E}_\ell^{ZX}(\rho)W_{\gamma_c}^{ZX\dagger} = \mathcal{E}_\ell^{ZX}(\rho)$ is satisfied. As we stated in the above, the operators $W_{\gamma_c}^{ZX}$ commutes with the stabilizers $\{W_v = A_v B_{v+\delta}\}$, and therefore the mixed state $\rho_f \propto \prod_v (1 + W_v)/2$ is 1-form weak symmetric; $W_{\gamma_c}^{ZX}\rho_f W_{\gamma_c}^{ZX\dagger} = \rho_f$. However, one should note that W^{ZX} symmetry is *not* a strong symmetry of ρ_f as $W_{\gamma_c}^{ZX}\rho_f \neq \rho_f$.

On the other hand, it is easily verified that the TC state ρ_{TC} is also weak symmetric for $W_{\gamma_c}^{ZX}$, i.e., $W_{\gamma_c}^{ZX}\rho_{\text{TC}}W_{\gamma_c}^{ZX\dagger} = \rho_{\text{TC}}$, which directly comes from the fact that the state ρ_{TC} satisfies the strong symmetry condition; $W_{\gamma_c}^{ZX}\rho_{\text{TC}} = \rho_{\text{TC}}$. The states ρ_{TC} and ρ_f reside on the fixed point of the 1-form weak symmetry W^{ZX} .

By the standard manipulation, we can introduce an anyon corresponding to the 1-form symmetry W^{ZX} by considering an operator $W_{\mathcal{C}}^{ZX}$, where \mathcal{C} is an open string and a pair of anyons emerge on endpoints of \mathcal{C} . We call this anyon f_w -anyon, which plays an important role for the discussion on the proliferation of anyon under decoherence as explained in the main text.

By following Ref. [37], one can study whether the W^{ZX} symmetry is spontaneously broken or not. To characterize the SSB of the 1-form weak symmetry of W^{ZX} , order and disorder parameters are to be used; the order parameter is given

by

$$C^I(\rho, \gamma'_c) \equiv \frac{\text{Tr}[\rho W_{\gamma'_c}^{X(Z)} \rho]}{\text{Tr}[\rho^2]},$$

where $W_{\gamma'_c}^{X(Z)} = \prod_{\ell \in \gamma'_c} X_\ell(Z_\ell)$ is a 't Hooft (Wilson) loop braiding nontrivially with $W_{\gamma_c}^{ZX}$.

On the other hand for the disorder parameter, the following Rényi-2 correlator is used,

$$C^{II}(\rho, (v_{e1}, v_{e2})) \equiv \frac{\text{Tr}[\rho W^{ZX}(v_{e1}, v_{e2}) \rho W^{ZX}(v_{e1}, v_{e2})]}{\text{Tr}[\rho^2]},$$

where the operator $W^{ZX}(v_{e1}, v_{e2})$ is defined similarly to the symmetry operator $W_{\gamma_c}^{ZX}$ supported along an open string with endpoints (v_{e1}, v_{e2}) as shown in Fig. 1(b) in the main text. As explained in the above, a pair of f_w -anyons are produced at v_{e1} and v_{e2} . As $W^{ZX}(v_{e1}, v_{e2})$ is commutative with all the stabilizers, f_w -anyon is a non-detectable anyon.

If the state ρ exhibits the 1-form Z_2 weak SSB (for W^{ZX}), then

$$C^I(\rho, \gamma'_c) = \mathcal{O}(1), \quad C^{II}(\rho, (v_{e1}, v_{e2})) = 0.$$

If not,

$$C^I(\rho, \gamma'_c) = 0, \quad C^{II}(\rho, (v_{e1}, v_{e2})) = \mathcal{O}(1).$$

In the main text, to characterize the IMTO numerically, we study the order and disorder parameters, $C^I(\rho, \gamma'_c)$ and $C^{II}(\rho, (v_{e1}, v_{e2}))$. In particular, in the stochastic ZX-decoherence channel, we observe the averaged susceptibility obtained from data of many samples.

2. Contractible loop W^{XZ} type of 1-form symmetry: By following Refs. [16, 17], another important 1-form symmetry is introduced, which is commutative with all the Kraus operators of the decoherence and also $W_{\gamma_c}^{ZX}$. The symmetry operator is given by $W_{\gamma_c}^{XZ} = \prod_{\ell \in \gamma_c} X_\ell Z_{\ell+\delta}$, where again, γ_c is a contractible closed loop on the q -lattice. It is easily verified that the channel \mathcal{E}^{XZ} is strong symmetric for W^{XZ} [34] due to $[W_{\gamma_c}^{XZ}, Z_\ell X_{\ell+\delta}] = 0$ for $\forall \ell$. The maximal decohered ZX state ρ_f exhibits the 1-form strong symmetry for $W_{\gamma_c}^{XZ}$, $W_{\gamma_c}^{XZ}\rho_f = \rho_f$ since $W_{\gamma_c}^{XZ}$ is given by a product of the stabilizers W_v [16, 17]. The TC state ρ_{TC} is also strong symmetric, i.e., $W_{\gamma_c}^{XZ}\rho_{\text{TC}} = \rho_{\text{TC}}$.

By following Ref. [37], there are measures to investigate whether the 1-form strong symmetry of $W_{\gamma_c}^{XZ}$ is spontaneously broken or not, that is, one can introduce the strong-SSB order and disorder parameters for $W_{\gamma_c}^{XZ}$ symmetry. The order parameter is given by

$$O_2(\rho) \equiv \frac{\text{Tr}[\rho W_{\gamma_c}^{X(Z)} \rho W_{\gamma_c}^{X(Z)} \rho]}{\text{Tr}[\rho^2]},$$

where $W_{\gamma_c}^{X(Z)} = \prod_{\ell \in \gamma_c} X_\ell(Z_\ell)$ is again a 't Hooft (Wilson) loop for a contractible loop γ_c , braiding nontrivially with

$W_{\gamma_c}^{XZ}$. On the other hand, the strong SSB disorder parameter is given as

$$D_1(\rho) \equiv \frac{\text{Tr}[\rho W^{XZ}(q_{e1}, q_{e2})\rho]}{\text{Tr}[\rho^2]},$$

where $W^{XZ}(q_{e1}, q_{e2})$ is an operator obtained from $W_{\gamma_{loop}}^{XZ}$ by restricting its support to an open string with endpoints labeled by q_{e1} and q_{e2} on the q -lattice. Similarly to the W^{XZ} 1-form symmetry, the above operator for an open string $W^{XZ}(q_{e1}, q_{e2})$ accompanies a pair of anyons at the endpoints q_{e1}, q_{e2} , which we call f_s -anyon in the main text. As $W^{XZ}(q_{e1}, q_{e2})$ anti-commutes with the stabilizers at q_{e1} and q_{e2} , f_s -anyon is a detectable anyon.

For the typical states ρ_{TC} and ρ_f , we can observe how the above order and disorder parameters for the strong 1-form XZ-symmetry behave. The maximal ZX-decohered state ρ_f is a SSB state of the 1-form strong symmetry since the 't Hooft and Wilson loops commute with all the stabilizers and the string operator $W^{XZ}(q_{e1}, q_{e2})$ cannot be given by a product of the stabilizers indicating $O_2(\rho_f) = 1$, $D_1(\rho_f) = 0$. It is similarly verified that the TC state ρ_{TC} is also 1-form strong SSB state since $O_2(\rho_{\text{TC}}) = 1$, $D_1(\rho_{\text{TC}}) = 0$.

Furthermore, one can study the properties of $W_{\gamma_c}^{XZ}$ as a 1-form weak symmetry. The order and disorder parameters are given as before,

$$O_1(\rho) = \frac{\text{Tr}[\rho W_{\gamma_c}^{X(Z)}\rho]}{\text{Tr}[\rho^2]},$$

$$D_2(\rho) = \frac{\text{Tr}[W^{XZ}(q_{e1}, q_{e2})\rho W^{XZ}(q_{e1}, q_{e2})\rho]}{\text{Tr}[\rho^2]}.$$

Let us observe the above quantities for the states, ρ_{TC} and ρ_f . For ρ_f ,

$$O_1(\rho_f) = 0, \quad D_2(\rho_f) = 0,$$

since $W_{\gamma_c}^{X(Z)}$ is not an element of the stabilizer group of the state ρ_f [$O_1(\rho_f) = 0$], and $W^{XZ}(q_{e1}, q_{e2})$ anti-commutes with the stabilizers W_v 's at the endpoints [$D_2(\rho_f) = 0$]. As both the order and disorder parameters are vanishing, we cannot judge if 1-form weak SSB for $W_{\gamma_c}^{XZ}$ symmetry takes place or not. We shall comment on this point later on.

On the other hand for the state ρ_{TC} ,

$$O_1(\rho_{\text{TC}}) = 1, \quad D_2(\rho_{\text{TC}}) = 0,$$

since $W_{\gamma_c}^{X(Z)}$ is a product of A_v 's or B_p 's, and the endpoint of $W^{XZ}(q_{e1}, q_{e2})$ anti-commutes with some A_v and B_p . Thus, the state ρ_{TC} is 1-form weak SSB for $W_{\gamma_c}^{XZ}$. In other words, the TC is a strong-trivial SSB state.

3. Comments on XZ-type 1-form symmetry with non-contractible loop: We can also introduce XZ-type 1-form symmetry with non-contractible loop. The generator is given by

$$W_{\gamma_{nc}}^{XZ} = \prod_{\ell \in \gamma_{nc}} X_\ell Z_{\ell+\vec{\delta}},$$

where γ_{nc} is a non-contractible loop on q -lattice. As this operator commutes with every Kraus operator, it remains a 1-form strong symmetry under the decoherence channel \mathcal{E}_ℓ^{ZX} . However, the ability of the logical operator is lost as its quantum conjugate operator such as the Wilson and 't Hooft non-contractible loop operators disappear from the stabilizer group under the channel \mathcal{E}_ℓ^{ZX} even if they are contained in the stabilizer group of the initial pure state. In other words, a transition from the genuine topologically ordered (TO) state to a state with classical memory takes place. More precisely, the proposed disorder parameters do not work for the non-contractible 1-form symmetry, because a finite length string is used in D_1 and D_2 .

4. Proposal of modified disorder parameter for XZ-type 1-form symmetry with detectable anyon: When an open string operator accompanies detectable anyon at endpoints (f_s -anyon in the current case) as in the 1-form strong W^{XZ} symmetry considered in the above, the disorder parameter $D_2 \sim \langle U_g(q_{e1}, q_{e2})\rho U_g^\dagger(q_{e1}, q_{e2})\rho \rangle$ is automatically zero because anyon is non-commutative with stabilizers at endpoints. [Its non-commutativity with stabilizers is the definition of the detectable anyon.] The order parameter of weak symmetry, O_1 , may also be zero, and in this case, it is unable to judge how the symmetry is realized in that state. In the current case, O_1 is zero for all possible U_h for the state ρ_f .

The disorder parameter is a measure how the state changes under the operation of the 1-form strong symmetry operator W^{XZ} applied in a subsystem. Its value is finite in the non-SSB state respecting symmetry as the state is not affected substantially by the symmetry operator W^{XZ} , whereas it is small in the SSB state as the state in the subsystem changes to another degenerate state. Reason why the disorder parameter vanishes when the detectable anyon resides on the endpoints of the string is physically obvious. Finite length string operator W^{XZ} accompanying a detectable anyon changes 'anyon state' of ρ to that of $U_g(q_{e1}, q_{e2})\rho U_g^\dagger(q_{e1}, q_{e2})\rho'$, which obviously makes the resultant state orthogonal to ρ because of a change in anyon sector in addition to the effects on the state along the string of W^{XZ} . Simple way to observe the genuine properties of the state is to remove the influence of the detectable anyon and examine a similar quantity to D_2 . In the fixed point state, it is easy to be done by removing the (non-commutative) stabilizer at the endpoints and calculate the same quantity. Formally we have a modified disorder parameter such as $D_2' \sim \langle U_g(q_{e1}, q_{e2})\rho' U_g^\dagger(q_{e1}, q_{e2})\rho' \rangle$, where ρ' is defined excluding the stabilizers that detect anyon at the endpoints of the string q_{e1}, q_{e2} . Specifically, in the current case, $\prod' (1 + W_v)$, where 'prime' indicates exclusion of a pair of W_v at the endpoints. Using this, the calculation suggests non-SSB with a finite D_2' for the 1-form strong symmetry W^{XZ} . Therefore, a strong-to-weak SSB state emerges due to the ZX-decoherence.

C. Numerical scheme

1. Update method for ZX decoherence in the stabilizer formalism: Some of decoherence channel can be implemented in the efficient stabilizer algorithm [42]. One example is a projective measurement without monitoring. We consider a local maximal decoherence corresponding to measurements with a local measure operator \hat{m}_i without monitoring (recording) the outcomes, where the label i refers to a relevant portion of the system. Here, we assume that \hat{m}_i is an element of Pauli group with +1 factor, and its measurement outcome denoted by β_i takes $\beta_i = \pm 1$. The channel is then given by

$$\mathcal{E}_i^{\hat{m}}[\rho] = \sum_{\beta_i=\pm} P_{\beta_i}^{m_i} \rho P_{\beta_i}^{m_i\dagger} = \frac{1}{2}\rho + \frac{1}{2}\hat{m}_i \rho \hat{m}_i,$$

where $P_{\beta_i}^{m_i}$ is a projection operator for \hat{m}_i with the outcome β_i given by $P_{\beta_i}^{m_i} = \frac{1+\beta_i \hat{m}_i}{2}$. If we apply the channel to an entire system with L degrees of freedom, the total channel is represented as

$$\mathcal{E}^{\hat{m}}[\rho] = \prod_{i=0}^{L-1} \mathcal{E}_i^{\hat{m}}[\rho].$$

Let us explain how the local channel $\mathcal{E}_i^{\hat{m}}$ acts to a mixed state in the stabilizer formalism. Here, we consider a density matrix represented by stabilizer generators $\{g_n\}$,

$$\rho = \frac{1}{2^{L-k}} \prod_{n=0}^{k-1} \frac{1+g_n}{2}, \quad (1)$$

where L is the total number of qubit in a system and k is the total number of independent stabilizer generators (generally, $k \leq L$). According to Ref. [42], the introduction of the local decoherence channel $\mathcal{E}_i^{\hat{m}}$ is efficiently implemented in the stabilizer algorithm. When one applies $\mathcal{E}_i^{\hat{m}}$ to ρ , then the state ρ becomes

$$\begin{aligned} \mathcal{E}_i^{\hat{m}}[\rho] &= \sum_{\beta_i=\pm} P_{\beta_i}^{m_i} \rho P_{\beta_i}^{m_i\dagger} \\ &= \sum_{\beta_i=\pm} P_{\beta_i}^{m_i} \left[\frac{1}{2^{L-k}} \prod_{n=0}^{k-1} \frac{1+\tilde{g}_n}{2} \right] P_{\beta_i}^{m_i\dagger} \\ &= \sum_{\beta_i=\pm} P_{\beta_i}^{m_i} \left[\frac{1+\tilde{g}_0}{2} \right] P_{\beta_i}^{m_i\dagger} \left[\frac{1}{2^{L-k}} \prod_{n=1}^{k-1} \frac{1+\tilde{g}_n}{2} \right] \\ &= \frac{1}{2^{L-k+1}} \prod_{n=1}^{k-1} \frac{1+\tilde{g}_n}{2}, \end{aligned}$$

where on the second line we have performed a standard transformation (corresponding to the change of the representation of the stabilizer generator) [32] to obtain other representation of $\{\tilde{g}_n\}$, in which at most one stabilizer generator labeled by \tilde{g}_0 is anti-commutative with \hat{m}_i . Thus, from the last line of the above equations, the application of the local channel

$\mathcal{E}_i^{\hat{m}}$ eliminates a single stabilizer generator from the set of stabilizer generators, leading to the enhancement of the mixing of the state. This procedure is directly implemented in numerical simulations.

2. Numerical calculation of negativity: We briefly explain how to calculate the negativity $N_A = \log_2 |\rho^{\Gamma_A}|_1$ defined in the main text. The original method calculating the negativity and its exact derivation are described in Refs. [41, 55]. As explained in Refs. [41, 55–57], the negativity N_A is practically obtained from a \mathbb{F}_2 matrix J

$$N_A = \frac{1}{2} \text{rank} J,$$

where J is a $m \times m$ matrix, m is the total number of the stabilizer generator for a state ρ in L total qubit system and here $m \leq L$. The matrix J is constructed from m -stabilizer generators g_n ($n = 0, \dots, m-1$) of the state ρ . Here, let us use the binary representation for g_n [32]. Then, we truncate the binary representation vectors of each stabilizer generator as

$$g_n \longrightarrow g_n^A = (g_0^{n,x}, \dots, g_k^{n,x} | g_0^{n,z}, \dots, g_k^{n,z}),$$

where $g_p^{n,x(z)} = 0$ or 1 and the binary components with the qubit label of the subsystem A (here labeled by $0, \dots, k$) remain. Finally, by using the m truncated stabilizer generators g_n^A , we construct the matrix J given by

$$(J)_{n,n'} = \begin{cases} 1 & \text{if } \{g_n^A, g_{n'}^A\} = 0 \\ 0 & \text{if } [g_n^A, g_{n'}^A] = 0 \end{cases},$$

where $\{g_n^A, g_{n'}^A\} = 0$ means that the truncated stabilizer generators g_n^A and $g_{n'}^A$ are anti-commuting, and similarly $[g_n^A, g_{n'}^A] = 0$ means that the truncated stabilizer generators g_n^A and $g_{n'}^A$ are commuting. By this manipulation, we obtain the binary $m \times m$ \mathbb{F}_2 matrix J . Finally, the calculation of the rank of J gives the value of negativity N_A .

3. Calculation method of C^I : We explain the numerical method for calculating the following quantity introduced in the main text,

$$C^I(\rho, \gamma'_c) = \frac{\text{Tr}[\rho W_{\gamma'_c}^Z]}{\text{Tr}[\rho^2]}.$$

If the operator $W_{\gamma'_c}^Z$ is a stabilizer obtained by a product of the stabilizer generators g_n of the state ρ , then $C^I(\rho, \gamma'_c) = 1$ since $W_{\gamma'_c}^Z \rho = \rho$. On the other hand, if the operator $W_{\gamma'_c}^Z$ is additional linearly dependent to all stabilizer generators of ρ , then $C^I(\rho, \gamma'_c) = 0$. Further, if the operator $W_{\gamma'_c}^Z$ is anti-commutative to at least one stabilizer generator of ρ , then $C^I(\rho, \gamma'_c) = 0$. These three cases are numerically judged by using the check matrix and the basic transformations of the set of stabilizer generators [32]. Thus, we can numerically calculate the value of $C^I(\rho, \gamma'_c)$.

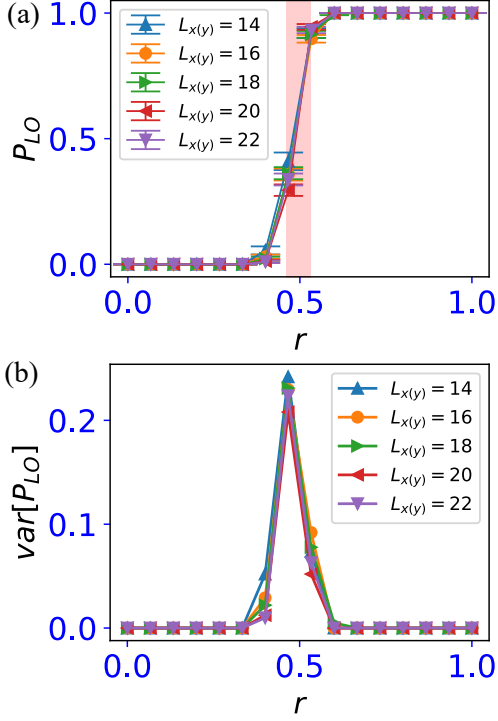


FIG. 4. (a) Annihilation probability of the logical operator of the TC state, $W_{\gamma^{x(y)}}^X$. (b) Variance of the annihilation probability obtained by averaging over samples of the trajectory.

4. Calculation method of Rényi-2 correlator: The Rényi-2 correlator such as $C^{\text{II}}(\rho, (v_{e1}, v_{e2}))$ in the main text can be calculated in the stabilizer formalism. We introduce an operator O_i . We assume that the operator O_i belongs to the Pauli group including identity with the factor +1 and a density matrix ρ is given by Eq. (1). Since each stabilizer generator g_n commutes or anti-commutes with the operator O_i , the Rényi-2 correlator for the density matrix ρ is given as

$$C_{O_i O_j}^{\text{II}}[\rho] = \frac{\text{Tr}[O_i O_j \rho O_j O_i \rho]}{\text{Tr}[\rho^2]},$$

and the numerator and denominator are calculated as

$$\text{Tr}[O_i O_j \rho O_j O_i \rho] = \frac{1}{2^L} \left[\prod_{n=0}^{k-1} (1 + \alpha^n) \right],$$

$$\text{Tr}[\rho^2] = \frac{1}{2^{L-k}},$$

with the factor $\alpha^n = \pm$ for $[O_i O_j, g_n]_{\pm} = 0$ (where $[\cdot]_{\pm}$ is commutative or anti-commutative bracket) and we have used $O_i O_j (1 + g_n) O_j O_i = (1 + \alpha^n g_n)$. Thus, we only extract the (anti)-commutativity between $O_i O_j$ and each stabilizer generator to obtain the Rényi-2 correlator.

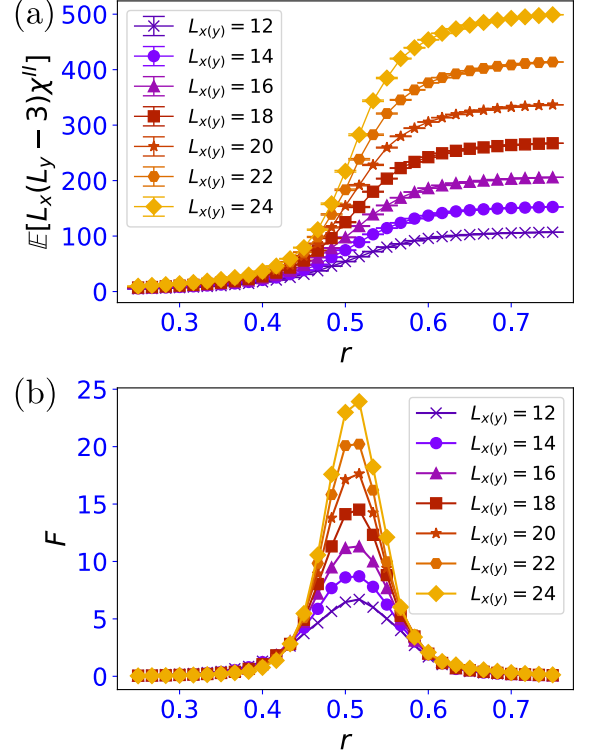


FIG. 5. (a) Behavior of $\mathbb{E}[L_x(L_y - 3)\chi^{\text{II}}]$ for different system sizes. (b) Rescaled variance F for different system sizes.

D. Annihilation probability of logical operator of toric code

As a supplemental observation, we numerically observe the fate of the logical operator of the TC $W_{\gamma^{x(y)}}^X$ by applying the stochastic ZX-decoherence channel discussed in the main text.

We prepare the pure unique TC state with the logical operators given by the set of the stabilizer generator, $S'_{\text{int}} = S_{\text{int}} + S_{X-\text{lg}}$. For a sparse ZX-decoherence corresponding to a small probability r , the logical operators can survive by deforming the loop $\gamma_{x(y)}$ due to applying star operator A_v 's. For a dense ZX-decoherence corresponding to a large r , the logical operator is strongly deformed and beyond a threshold, it is to be swept away from the set of the stabilizer generator, indicating vanishing of the TC phase. We numerically trace the existence of the logical operators under the numerical update in the efficient stabilizer update algorithm and estimate the annihilation probability of the logical operators denoted by P_{LO} as varying the probability r (A similar calculation for a pure state case has already been demonstrated in [58]). Figure 4(a) is the behavior of P_{LO} obtained by averaging over trajectories. P_{LO} suddenly increases around $r = 0.5$ consistent with the numerical results shown in the main text, that is, the topological order of the TC state is swept indicating the change of the mixed state in this stochastic circuit. Finally, the

variance of P_{LO} obtained by the fluctuation of the trajectory samples is shown in Fig. 4(b). The peak is observed around $r = 0.5$, indicating the mixed state phase transition in the level of the averaged trajectory picture.

E. Rescaled χ^{II} and its rescaled variance

Here we show the ensemble average of the rescaled χ^{II} , denoted by $\mathbb{E}[L_x(L_y - 3)\chi^{\text{II}}]$ as varying r in Fig. 5(a). The entire value is getting larger as increasing the system

size. Furthermore, we obtain its variance σ from many samples of $(L_x(L_y - 3)\chi^{\text{II}}(\rho_s, r))$ with various system sizes $[\text{var}[L_x(L_y - 3)\chi^{\text{II}}]]$. We then observe a rescaled variance $F \equiv \sigma/(L_x(L_y - 3))$ as shown in Fig. 5(b). The peaks for different system sizes locate around $r = 0.5$ and the value of the peak gets larger as increasing the system size. By using this data, we carry out the scaling analysis and obtain the scaling function (indicating the clear data collapse) as shown in the inset of Fig. 3(b) in the main text.